THE DEATH OF A MID-LEVEL CLOUD

Vincent E. Larson[1] [*], Robert P. Fleishauer[2], J. Adam Kankiewicz[2], Donald L. Reinke[2], and Thomas H. Vonder Haar[2]

[1] Atmospheric Science Group, Dept. of Mathematical Sciences, University of Wisconsin — Milwaukee, Milwaukee, Wisconsin.

[2] Cooperative Institute for Research in the Atmosphere, Colorado State University, Fort Collins, Colorado.

1. INTRODUCTION

Altocumulus clouds reside in the mid troposphere, contain rounded and often convective elements, and are thin (on the order of 100 meters) (Heymsfield 1993).

The physics of altocumulus clouds is distinctive in several ways. First, unlike many boundary layer clouds, altocumuli cannot be maintained by surface moisture fluxes. This fact naturally shifts attention from the steady state problem to the decay problem. Second, large-scale vertical velocity is a stronger forcing on mid-level clouds than on boundary layer clouds, because vertical velocities become small near the ground. Third, unlike midlatitude or tropical boundary layer clouds, mid-level clouds are often mixed phase (Fleishauer et al., Observed Microstructure of Mid-Level, Mixed-Phase Clouds, submitted to *J. Atmos. Sci.*, 2001).

Altocumulus clouds are of practical interest for several reasons. First, altocumuli impede pilots' visibility and thereby hamper military operations (Fleishauer et al., 2001). Second, changes in anthropogenic aerosols may change the albedo (Twomey 1974) and emissivity (Garret et al., Aerosol Effects on Cloud Emissivity and Surface Longwave Heating in the Arctic, submitted to *J. Atmos. Sci.*, 2001) of altocumulus clouds, thereby influencing the climatic radiation balance. Third, altocumuli are ubiquitous. Despite the importance of these clouds, there have been relatively few reports of in-situ altocumulus measurements (exceptions include Hobbs and Rangno 1985; Heymsfield et al. 1991; Heymsfield 1993; and Hobbs and Rangno 1998).

In this paper we analyze aircraft measurements of an altocumulus cloud over Montana on 11 November 1999. The aircraft arrived during the decay phase and continued sampling until the cloud disappeared (see Figure 1). When the measurements commenced, the cloud extended vertically from 5180 m (-13 C) to 5705 m (-17 C), had a cloud fraction of unity, and covered an area of about 6000 km^2. The cloud was mixed phase but was predominantly liquid (see Figure 2). See Fleishauer et al. (2001) for more details of this cloud and a description of the aircraft instrumentation.

What caused the decay of this mid-level cloud? There are four possible culprits: large-scale subsidence, radiative heating, entrainment drying, and precipitation fall-

out. This paper estimates which of these processes contributed most. To do so, we construct a budget of the vertically averaged specific liquid water content, $\langle q_l \rangle$. The budget helps elucidate whether the lifetime of the November 11 altocumulus cloud was limited by microphysics or dynamics.

2. BUDGET OF LIQUID WATER

Because ice water content was small (Figure 2) and had little effect on radiative cooling, our budget neglects ice except insofar as it removes liquid via precipitation. The time rate of change of $\langle q_l \rangle$ is affected by four terms:

$$\frac{d \langle q_l \rangle}{dt} = \text{Subs} + \text{Entr} + \text{Rad} + \text{Precip.} \qquad (1)$$

We assume that the cloud was saturated with respect to liquid water. Then subsidence drying is given by

$$\text{Subs} = \left(\frac{\partial q_l}{\partial p} \right)_{\theta_l, q_t} w \frac{dp}{dz}, \qquad (2)$$

where w is the cloud-averaged vertical velocity of air, p is pressure, θ_l is liquid water potential temperature, and q_t is total specific water content, which includes vapor and liquid but not ice. Entrainment drying is given by

$$\text{Entr} = \left(\frac{\partial q_l}{\partial q_t} \right)_{\theta_l, p} \frac{w_e \Delta q_t}{h} + \left(\frac{\partial q_l}{\partial \theta_l} \right)_{q_t, p} \frac{w_e \Delta \theta_l}{h}, \qquad (3)$$

where $w_e > 0$ is the entrainment velocity, h is cloud depth, Δq_t is [q_t just above cloud top] minus [q_t just below cloud top], and $\Delta \theta_l$ is the analogous difference for θ_l. The radiative cooling term is

$$\text{Rad} = \left(\frac{\partial q_l}{\partial \theta_l} \right)_{q_t, p} \left(\frac{p_0}{p} \right)^{R_d/c_{pd}} \dot{Q}, \qquad (4)$$

where $\dot{Q}$ is the radiative cooling rate, p_0 is a reference pressure, R_d is the gas constant for dry air, and c_{pd} is the specific heat at constant pressure of dry air. Loss of water via precipitation of ice crystals is given by

$$\text{Precip} = \frac{\sum_i N_i m_i v_{t,i}}{\rho_a h}, \qquad (5)$$

where N_i is number concentration of ice crystals in the ith bin, m_i and $v_{t,i}$ are the mass and terminal velocity of a crystal in the ith bin, and ρ_a is the density of air.

---

[*]*Corresponding author address:* Vincent E. Larson, Department of Mathematical Sciences, University of Wisconsin — Milwaukee, P. O. Box 413, Milwaukee, WI 53201-0413; e-mail: vlarson@uwm.edu
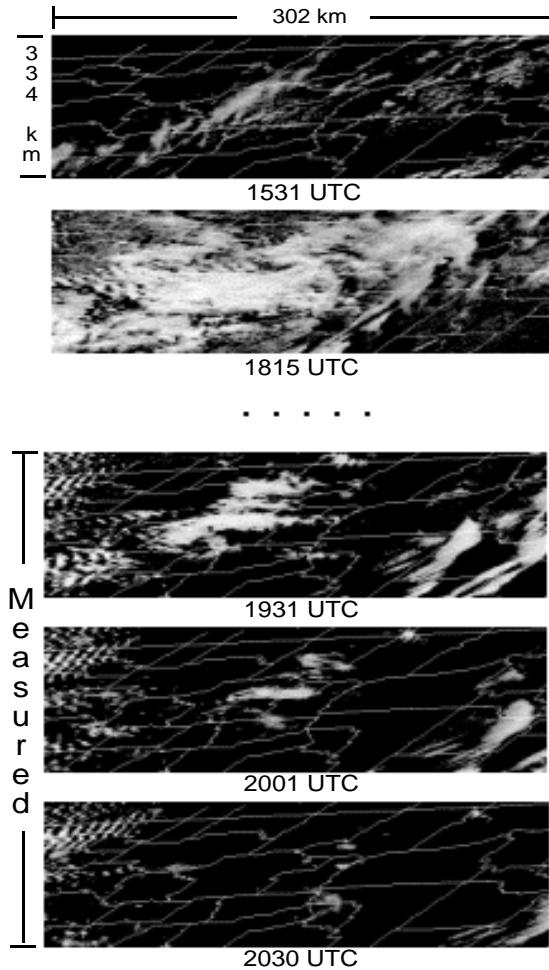
302 km

3 3 4 k m

1531 UTC

1815 UTC

. . . . .

M e a s u r e d

1931 UTC

2001 UTC

2030 UTC

Figure 1: A series of GOES-8 visible satellite images of the 11 November 1999 cloud.

3. METHODS USED TO EVALUATE TERMS IN LIQUID WATER BUDGET

The above terms in the budget are evaluated using aircraft data and numerical models as follows.

3.1 Horizontal advection

The flight pattern consisted of a spiral sounding followed by a series of racetrack-shaped patterns at different altitudes. While executing this pattern, the aircraft drifted with the horizontal wind (Fleishauer et al., 2001). Since the racetracks followed a column of air in a Lagrangian sense, we can assume that measured changes in liquid water reflect temporal changes following a column of air, not spatial inhomogeneity. Therefore our budget omits the horizontal advection term.
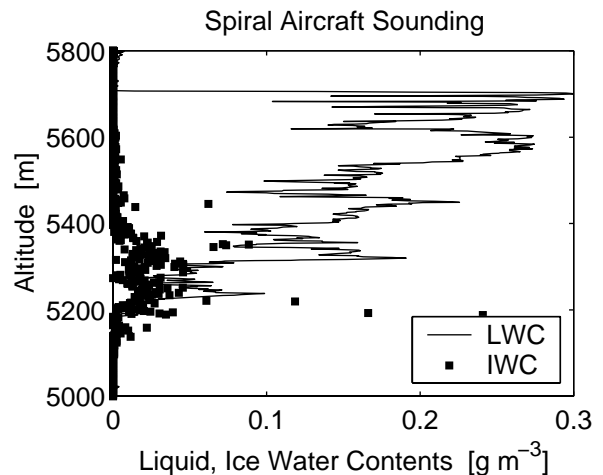

Figure 2: Profiles of liquid and ice water content as measured by the King probe and 2D-C probe, respectively.

3.2 Entrainment

To compute the entrainment velocity, w_e, we use the flux-jump method: that is, we set $w_e = -\overline{w'q_t'}/\Delta q_t$, where $\overline{w'q_t'}$ is the turbulent flux of q_t just below cloud top. Since there was no detectable jump in θ_l or q_t at the base of the cloud, we can neglect entrainment into the base. To compute $\overline{w'q_t'}$, we use two legs of a racetrack that occurred 100 m below cloud top. We condition the data following Bretherton et al. (1995) and Stull (1988, pp. 308–310). Then we find that for the first leg (14.2 km), $w_e = 1.1$ cm s^{-1}, and for the second leg (15.26 km), $w_e = 0.75$ cm s^{-1}. Uncertainty of up to a factor of two is introduced by poor sampling due to the short leg lengths (see Lenschow and Kristensen 1985). In the liquid water budget below, we use the average of w_e over both legs, namely, 0.9 cm s^{-1}.

3.3 Precipitation

Sedimentation from cloud base occurred in the form of ice crystals of several hundred microns diameter. The Cloud Particle Imager (CPI) revealed that these particles were typically unrimed broad-branched crystals (P1c), although some crystals were needle-shaped and/or lightly rimed. We compute precipitation rate using 2D-C data obtained from four within-cloud aircraft legs near cloud base (named 2a, 2b, 7a, 7b). Using the ice crystal mass and terminal velocity formulation of Mitchell (1996), we find that the maximum precipitation rate is from leg 7a (4.4×10^{-7} kg m^{-2} s^{-1}), the minimum is from leg 7b (2.9×10^{-9} kg m^{-2} s^{-1}), and the average over all four legs is 1.3×10^{-7} kg m^{-2} s^{-1}. This gives a sense of the uncertainty due to sampling error. Uncertainty in the precipitation rate is also introduced by the mass and terminal velocity formulations. If we follow Kajikawa (1989), we find an average precipitation rate that is almost four times larger (3.9×10^{-7} kg m^{-2} s^{-1}). In the liquid wa-

ter budget below, we use the average precipitation rate as computed by Mitchell (1996). Finally, uncertainty is introduced by the fact that the 2D-C probe cannot detect precipitating particles larger than 1056 microns in diameter, and a few particles larger than this were seen in the CPI imagery. However, we estimate that missed particles lead to a precipitation underestimate of at most a factor of two. We perform this estimate by smoothly extrapolating the ice spectrum to large sizes using the assumption of an exponential ice number concentration.

3.4 Radiative cooling

To obtain the cloud-averaged heating due to solar and infrared radiation, we use a new two-stream radiative transfer model (Stephens et al., Parameterization of Atmospheric Radiative Transfer: I. Validity of Simple Models, submitted to *J. Atmos. Sci.*, 2000). As input, we use the aircraft liquid and ice profiles merged with a routine radiosonde sounding launched from Great Falls, Montana at 0 UTC 12 November 1999. The net total cloud-averaged heating rate is -7.6×10^{-5} K s^{-1}. This value changes by about 15% if the liquid water is doubled or halved everywhere.

3.5 Large-scale subsidence

Large-scale subsidence tends to warm a mid-level cloud and hence deplete its liquid water. To estimate large-scale vertical velocity, we use a numerical model, as in Bretherton et al. (1995). Specifically, we use a University of Utah MM5 forecast that was initialized at 1200 UTC 11 November 1999 and run at 36-km horizontal grid spacing.

When the cloud formed ($\sim$1500 UTC), the air motion was upward at several cm s^{-1}. From the middle (1800 UTC) to the end of the cloud's lifetime, the vertical velocity was downward at about -3 cm s^{-1}. See Figure 3(a),(b), and (c).

Why do we see gentle upward then gentle downward motion? This pattern appears to have been associated with an upper tropospheric patch of high potential vorticity (PV) that formed near a trough and advected eastward over Montana (see Figure 3(d),(e),(f)). Beneath a high PV anomaly, isentropes bow upward. Therefore, as high PV aloft approaches from the west, a mid-level parcel below rises along an isentrope. Later, as the PV patch moves off to the east, the parcel sinks back to nearly its original altitude (Hoskins et al. 1985).

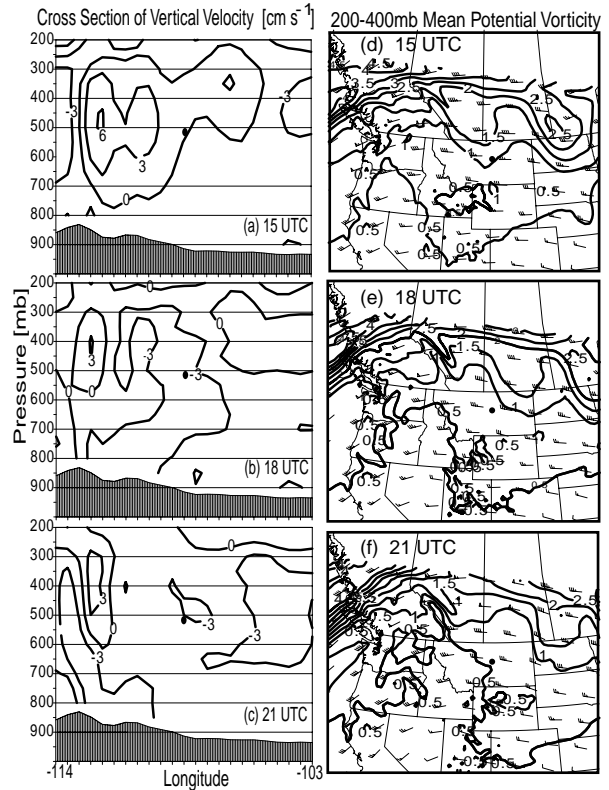|	Liquid decay rate [kg kg^{-1} s^{-1}]	(Term decay rate)/ (Subsid. decay rate)
Subsidence	-3.3×10^{-8}	1.0
Entrainment	-1.5×10^{-8}	0.44
Radiation	+1.0×10^{-8}	-0.30
Precipitation	-3.6×10^{-10}	0.011

Table 1: Terms in Liquid Water Budget

Figure 3: Output from an MM5 forecast initialized at 12 UTC 11 November 1999. Panels (a), (b), and (c) show a cross section of vertical velocity. The dot indicates cloud location during the middle of the measurement period, about 20 UTC 11 November 1999. Panels (d), (e), and (f) show a latitude-longitude plot of isentropic potential vorticity, averaged over a layer from 200 mb to 400 mb. The dot in the center of Montana indicates cloud location at 20 UTC 11 November 1999. Contours are in PV units. A large wind barb denotes 10 m s^{-1}. As the PV patch passes over central Montana, the mid-level cloud first rises and then subsides.

4. DISCUSSION OF MAGNITUDE OF TERMS IN LIQUID WATER BUDGET

Our main results are shown in Table 1, which lists the rate at which each of the four aforementioned processes tends to deplete liquid water. If we account for all four processes, assume that liquid water decreases at a constant rate, and take the initial liquid water content to be the vertical average of the aircraft sounding, then we calculate a decay time of 88 minutes. This is consistent with the observed decay time between the aircraft sounding and the death of the cloud (74 minutes).

The largest term is subsidence drying. The magnitude of the model-produced vertical velocity (-3 cm s^{-1}) is corroborated by the fact that this subsidence rate is consistent with the observed decay time and the other terms in the liquid water budget.

The next two largest terms are entrainment, which tends to dry the cloud, and radiation, which tends to cool the cloud and hence increase liquid water. To a large degree, these two terms offset each other. This is interesting because in this cloud it was radiation, not shear, that generated turbulence and hence entrainment (Fleishauer et al., 2001). Therefore, radiation increases liquid water by direct cooling but decreases liquid water by radiatively induced entrainment. This is further complicated by the fact that entrainment causes cloud top to rise, cool, and hence experience increased liquid water. Given the uncertainty in our measurements, it is not obvious whether the net effect of radiation was to prolong or curtail the lifetime of our cloud.

By far the smallest term is precipitation drying. This is somewhat surprising, because virga were observed, and the cloud top height decreased rapidly at the end of the cloud lifetime, possibly due to precipitation. However, even assuming imperfect measurements, it is unlikely that the precipitation term exceeded 20% of the subsidence term.

5. CONCLUSIONS

The picture that emerges is that the evolution of our cloud was governed primarily by large-scale ascent and then subsidence. Because radiation and entrainment in our altocumulus partially offset each other, and because precipitation was weak, we would have obtained a similar cloud decay time if we had ignored all terms except subsidence.

Subsidence limited the lifetime of our altocumulus cloud because the subsidence rate at mid-levels was large (~ 3 cm s^{-1}). A smaller subsidence rate is usually associated with boundary layer clouds. For instance, subsidence rates during the Atlantic Stratocumulus Transition Experiment Lagrangians were $\overset{\sim}{<} 1$ cm s^{-1} (Bretherton et al. 1995).

It would be rash to generalize on the basis of a single case study. Nevertheless, our results provide preliminary guidance for development of numerical models and future field experiments. Namely, if altocumulus lifetime is of interest, and if the lifetime is governed primarily by subsidence, then special attention should be devoted to the large-scale velocity and moisture fields. In contrast, past observational studies of altocumuli have focused more on microphysics.

There is also a possible implication for the second indirect effect or cloud lifetime effect, in which an increase in aerosols leads to less precipitation and hence longer cloud lifetime. If it turns out that altocumulus lifetime is usually limited by subsidence rather than precipitative fallout, then the cloud lifetime effect for altocumuli may be small.

6. REFERENCES

Bretherton, C. S., P. Austin, and S. T. Siems, 1995: Cloudiness and marine boundary layer dynamics in the ASTEX Lagrangian experiments. Part II: cloudiness, drizzle, surface fluxes, and entrainment, *J. Atmos. Sci.*, **52,** 2724-2735.

Heymsfield, A. J., L. M. Milosevich, A. Slingo, 1991: An observational and theoretical study of highly supercooled altocumulus, *J. Atmos. Sci.*, **48,** 923-945.

Heymsfield, A. J., 1993: Microphysical structures of stratiform and cirrus clouds, in *Aerosol-cloud-climate interactions,* edited by P. V. Hobbs, pp. 97-121, Academic Press, San Diego, CA.

Hobbs, P. V., and A. L. Rangno, 1985: Ice particle concentrations in clouds, *J. Atmos. Sci.*, **42,** 2523-2549.

Hobbs, P. V., and A. L. Rangno, 1998: Microstructures of low and middle-level clouds over the Beaufort Sea, *Q. J. R. Meteorol. Soc.*, **124,** 2035-2071.

Hoskins, B. J., M. E. McIntyre, and A. W. Robertson, 1985: On the use and significance of isentropic potential vorticity maps, *Q. J. R. Meteorol. Soc.*, **111,** 877-946.

Kajikawa, M., 1989: Observation of the falling motion of early snowflakes. Part II: On the variation of falling velocity, *J. Meteor. Soc. Japan*, **67,** 731-737.

Lenschow, D. H., and L. Kristensen, 1985: Uncorrelated noise in turbulence measurements, *J. Atmos. Oceanic Technol.*, **2,** 68–81.

Mitchell, D. L., 1996: Use of mass- and area-dimensional power laws for determining precipitation particle terminal velocities, *J. Atmos. Sci.*, **53,** 1710-1723.

Stull, R. B., 1998: *An introduction to boundary layer meteorology,* 666 pp., Kluwer Academic Publishers, Norwell, MA.

Twomey, S., 1974: Pollution and the planetary albedo, *Atmos. Environ.*, **8,** 1251-1256.